Personalized Fitting of Respiratory Mask Using 3D Numerical Simulation and Finite Element Analysis

Hugo TAECKENS [*1], Arthur AGOSTINI [1], Loïc DEGUELDRE [2], Bahe HACHEM [2],
Sean-Philippe VIENS [3], Aude CASTONGUAY-HENRI [3], Jonathan BORDUAS [3], Luc DUONG [1]
[1] École de Technologie Supérieure, Montréal (QC), Canada;
[2] Numalogics, Montréal (QC), Canada;
[3] ShapeShift 3D, Montréal (QC), Canada

https://doi.org/10.15221/22.48

Abstract

Respiratory masks, such as N95, are widely used in clinical and industrial environments because of their high filtration capacity. However, prolonged wear could provide discomfort due to poor fitting to each individual's face's exact morphology and excessive tightening.

This study aims to personalize the design of respiratory masks and simulate the fitting using finite element analysis. A cohort of 7 participants was recruited to evaluate the fit of a virtual 3D mask. A scan of the face was performed on an iPhone by an app using ARKit to acquire a geometric model for simulation.

The mask pressure and seal were calculated digitally using Ansys Mechanical after importing the 3D geometries of the mask and the face. An algorithm allows to place the mask in front of the face without inter-penetration. Facial soft tissues were accounted as a homogeneous hyperelastic material model. The silicone was modeled using hyperelastic material properties and the mask was considered as rigid. A pressure map illustrates the pattern that the mask will produce on a given user's face, in order to assert the desired comfort criteria. A map of the gap between the mask and the face shows the sealing capability of the mask. The pressure points of the silicone on the face were simulated after tightening the mask. The pressure pattern must be uniform and without pressure peaks to ensure user comfort.

To ensure the consistency of the numerical results, experimental pressure measurements were also performed on the participants and their dedicated masks. Facial pressure calculation and measurement tests were performed under 3 levels of tightening (low = 5N, medium = 13N and high = 20N).

The outcome of this study could provide major insights in the design of respiratory masks through face scanning technologies and numerical simulation. Moreover, it could contribute to fully customize the respiratory mask to the user's face, for enhanced comfort and proper sealing.

Keywords: respiratory mask, custom fit, face scanning, finite element analysis, numerical simulation

1. Introduction

First and foremost, respiratory protection is necessary in workplaces with a context conducive to the development of respiratory diseases by inhalation of harmful dusts, particles, or gases. The main risks are the development of asthma, acute inhalation injury or lung cancer for example [1,2].

Respiratory protection became common during the COVID-19 pandemic recognized in January 2020 by the World Health Organization (WHO). The virus is transmitted mainly by respiratory droplets (> 5-10µm) during close contact (approximately < 1.80m) with another individual, especially when the latter coughs or sneezes [3,4,5,6].

To deal with contamination in both industrial and medical environments, the use of protective devices such as respiratory masks, dust masks and other equipment is essential.

One of the most common types of protection is the N95 respirator. It is widely used in both medical and industrial environments because of its high filtration capacity: 99.5% for particles larger than 0.75µm and 95% (smallest filtration) for particles between 0.1 and 0.3µm [7,8,9]. However, users report a high lack of comfort, especially for long-term wear [10]. Breathing and speaking are also a problem. These masks, if they are too tight over a prolonged period, create too much pressure on the skin of the face and can cause problems of skin irritation. This is especially true around the nasal area [11]. There is therefore a strong demand for new high-performance and comfortable breathing masks.

ShapeShift 3D has then designed a custom mask adapted to the morphology and shape of a user's face. A scan of the face is performed by an application on a smartphone and will allow the creation of the mask's geometry. The goal of this study is to assess mask performance using numerical simulation by finite element analysis. To ensure the consistency of the numerical results, experimental pressure and gap measurements were also performed on the participants and their dedicated masks. Facial pressure calculation and measurement tests were performed under 3 levels of tightening (low = 5N, medium = 13N and high = 20N).

This paper is organized as follows: in section II, we first present the steps for creating the mask. The determination of the pressure by finite element simulation is also presented in this section. This numerical pressure model is then confirmed by experimental tests on the participants. The pressure and gap values by simulation and experimental measurements are presented in section III. Section IV discuss the results and limitations. It also describes the future use of Artificial Intelligence to replace the simulation, to provide the fit results in real-time as the customer establishes their mask order.

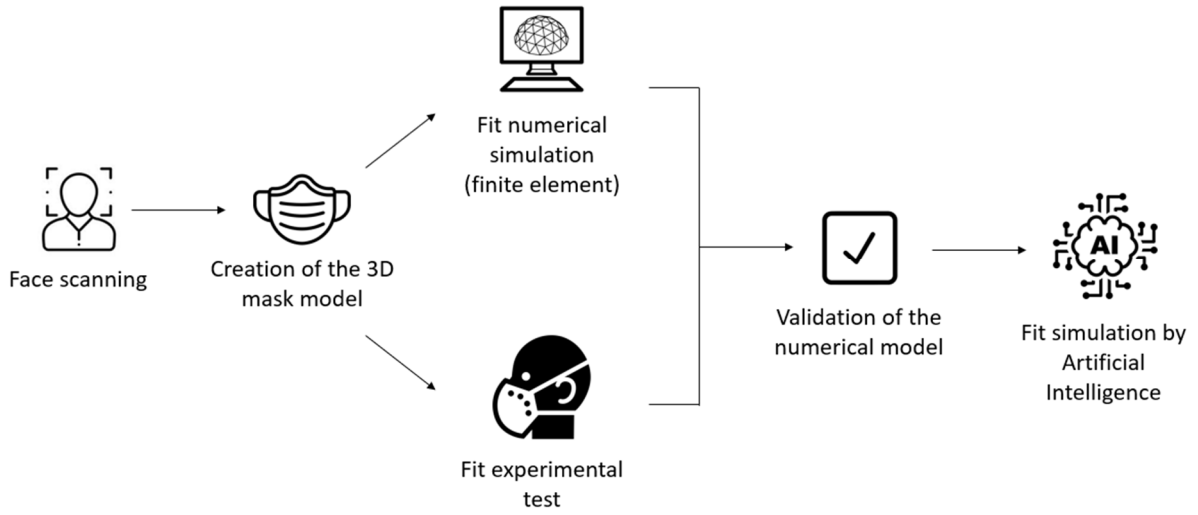

Fig. 1. Protocol for mask fit simulation. After the face scan by smartphone, the geometry of the personalized breathing mask is created. The pressure and seal results from the simulation (finite element method) are compared with the experimental results to validate the model. When the model is validated, these characteristics will be determined by Artificial Intelligence.

2. Materials and methods

2.1. Acquisition of the 3D profile and creation of the mask geometry by face scanning.

The process of creating the mask involves several steps. The face is first scanned by ShapeShift3D's proprietary *We3D* application. This application uses the ARKit scanning technology available on Apple smartphones. The justification of the scanning technique was detailed in [12]. According to the authors, ARKit scans achieve good accuracy (Interclass Coefficient Correlation (ICC) = 0.94 ± 0.08) and is user-friendly as it does not require an experienced external person. The mesh of the face obtained by ARKit has also the advantage of presenting the same architecture between all the faces, so landmarks are consistent and easily identified between 2 scans. However, the scanned geometries are smoothed and much less detailed than other alternatives, especially on the cheeks. Also, with this application, only the face is scanned (fig.2): the rest of the jaw, the neck, and the back of the head are reconstructed by AI.

For this study, another scanning technique has been used, which uses a Structure Sensor (Occipital, Boulder, Colorado, USA). The device is attached to the iPad, and, unlike We3D, this application captures the entire face. It also requires a trained external person to realize the scan. The goal was to establish and qualify the scan bias between ARKit and the Structure Sensor (study conducted by ShapeShift).

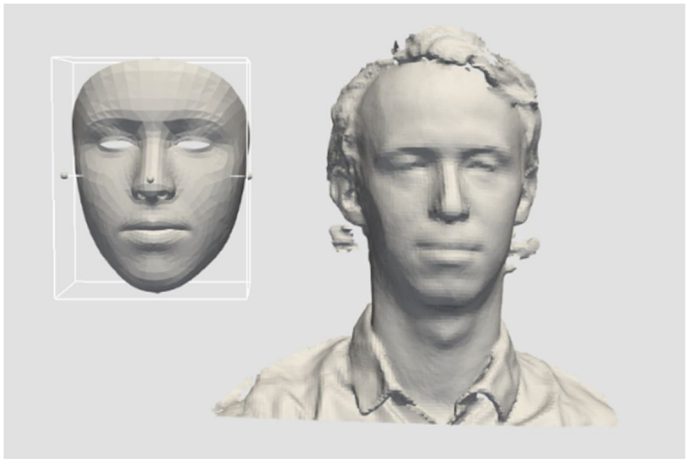

Fig. 2. Face scan with We3D (left), and with Structure Sensor (right)

2.2. Pressure quantification created by the mask via Finite Element Analysis

To quantify the pressure created by the mask on the face, numerical simulation and more particularly Finite Element Analysis has been used. This method is widely used by mechanical engineers and is based on a volumetric and continuous model of the material, which is cut into a mesh of elements. It is on each of these elements that it is possible to linearize the partial differential equations governing the global deformation of the structure, by a system of linear equations. We decided to use the software ANSYS (ANSYS Inc., Canonsburg, Pennsylvania, USA) to run the simulation. Most of the simulation parameters have already been presented in [13] but were further refined for the current study.

Finite element simulations are used to obtain the results of the mask pressure on the face in MPa. The sealing criterion is obtained by calculating the distance between the mask and the face. If this distance is not zero around the face, then there is a leak, and the seal is not perfect.

The geometric 3D models of the adapted faces and masks are imported into Ansys Mechanical. An algorithm is used to iteratively place the mask in front of the face without inter-penetration. Facial soft tissues were accounted as a homogeneous hyperelastic material model. The silicone was modeled by the hyperelastic material [Martins2006] and the mask is considered as rigid. The back and bottom of the head are considered fixed. The back of the head is considered frictionless, with permitted finite sliding. Pilot simulations identified a friction coefficient between the skin and the silicone of 0.4, below the values found in the literature [14] but within their reported range.

Pre-Pilot tests and values found in the literature [15] indicated that tightening forces beyond 20N result in a discomfort on a small sample of subjects. Thus, 20N was selected as the tightening limit with low and moderate values reflecting 5N and 13N.

Contrary to what was presented in [13], the tightening is no longer done by a force of 20N on the polyamide parts of the mask. This has been replaced by a spring attached to the center of the mask, which gradually contracts to a restoring force equivalent to the tightening force. Such a modelling strategy allows the mask to freely move and adapts its position to the face’s geometry.

These pressure calculations are performed on each scan from the 2 technologies (ARKit and Structure Sensor), with the corresponding mask.

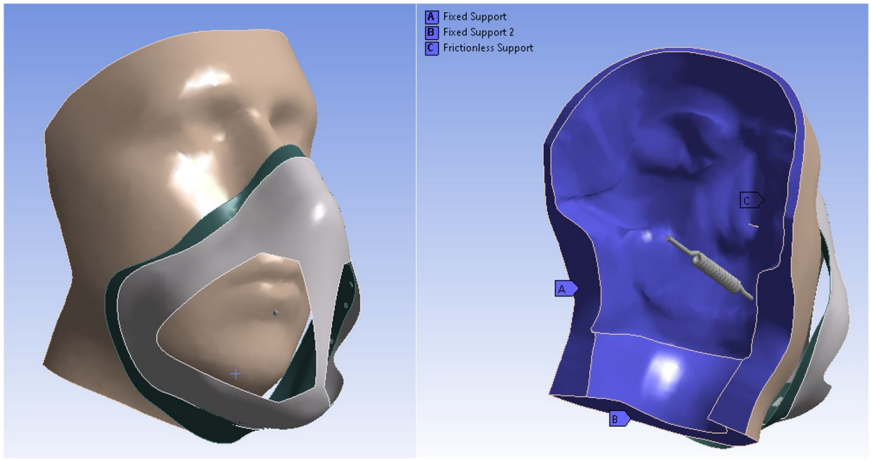

Fig. 3. Face and mask model on Ansys Mechanical, with the tightening spring and the limit conditions

2.3. Validation of the numerical model by experimental tests

2.3.1. Measurement of the tightening force

To confirm this finite element pressure calculation model, the actual pressure is measured experimentally. For each participant, the pressure on the face of each of their fitted 2 masks (ARKit and Structure Sensor) is measured for each of the 3 tightening forces. No studies or data have been done on the tightening force of masks to our knowledge. We therefore had to create our own instrumented system.

First, the tightening device provided with the mask was removed (tightening straps + strap at the back of the head). On each side of the mask, a spring of 2" empty length, 4.5lbs maximum load and 2lbs/in stiffness was attached. A ruler was designed, and 3D printed. It is attached in parallel to the springs to protect the skin and to measure the spring's elongation. At the back of the skull, a bicycle helmet roller tightening straps were retrofitted on the mask (see figure 4). During the tightening, the springs will lengthen. The measurement of the elongation is done directly with the ruler. The tension force of each spring corresponds to half of the mask tightening tension (springs in parallel) and can then be determined from the spring stiffness. The roller tightening device was used to finetune the tightening process by correlating the applied tension to "tightening the roller by one notch".

Fig. 4. Instrumented mask (without filter cartridges) for measuring tightening force. The bicycle helmet tightening device makes it easier to manage the tightening of the mask. When the mask is tightened, the springs on the sides (in the white rulers) will stretch and knowing the characteristics and the elongation, the return force of the spring can be deduced (which is equal to the tightening force).

2.3.2. Pressure experimental determination

The pressure is measured with SingleTact Miniature Force Sensors (SingleTact, Glasgow, UK). They are capacitive force sensors and were chosen for their superior sensitivity and repeatability compared to resistive sensors. They are only 0.30mm thick, which is very important to us to reduce the geometric interference of the scanner on the measured pressure. A 15mm diameter and 45N force calibrated sensor was selected as equivalent measured pressures lied within the expected reported face-mask pressures [15]. The advantage of using calibrated sensors versus non calibrated is that they offer ever more superior accuracy and linearity compared to standard ones. The relation between the applied force (in Newton) and the voltage output (in Volt) is linear with these sensors, which directly provides the force applied to the sensor.

2.3.3. Seal experimental determination

Quantitative fit and seal testing of the masks has been carried out by ShapeShift to achieve NIOSH certification. Our aim here is therefore more qualitative than quantitative, in particular to visualize the contact points of the silicone on the mask and ensure consistent contact along the contour of the mask-face interface. To ensure that the mask-face interface is sealed, white makeup was applied to the participant's face while black makeup was applied on the mask's silicone. The makeup used was purchased in a costume store (Halloween type), is non-allergenic, and can easily be removed with soap and water without leaving any traces. The mask is carefully applied with the average tightening force. The areas of the face where makeup has been deposited correspond to a silicone/skin contact and therefore correspond to a seal. On the other hand, in the areas where the make-up has not been deposited, the mask does not touch the skin and there is therefore a leak.

3. Results

The faces of 7 different people were scanned according to the procedure explained in 2.1 to obtain first results. The 7 people are male, aged between 25 and 45 years and have white skin.

3.1. FEM analysis

Figure 5 shows the pressure and tightness results for one randomly selected subject from the 7 randomly participants (subject 6). Each simulation took around half an hour to run on 6-cores.

On this person, the pressure is relatively evenly distributed across the face, with areas of greater pressure on the nose (orange circle, Fig.5A.), upper cheeks (red circle, Fig.5B.), and on the neck below the chin (yellow circle, Fig.5C.). The maximum pressure applied by the mask is $5.330.10^{-2}$ MPa at the top of each cheek. There is a sealing problem at the nose (green circle, Fig.5E.), with a gap of up to 3mm. The results are globally symmetrical between the two sides of the face, which was not the case in [11]. A gap of up to 3mm is present at the nose, which was present in all simulations. The value of -3mm as a threshold value for leakage was taken from [16].

The following graph shows the maximum pressure on all faces. The pressure points were of the same order of magnitude and appear in the same anatomical structures (nose, top of the cheeks and below the chin)

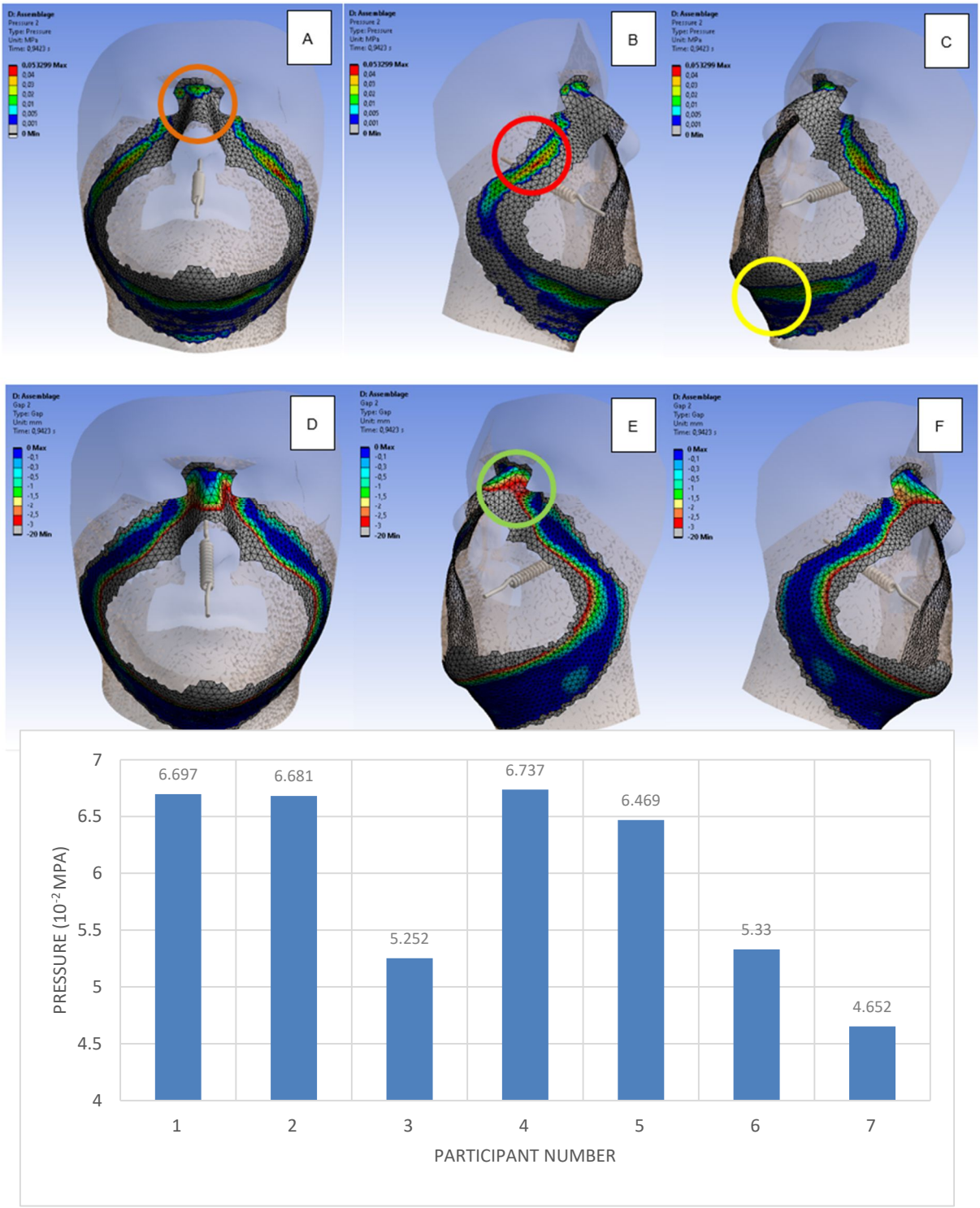

Fig. 5. Pressure (MPa) on the face of subject 6 (top); Gap (blue color = seal) between silicon shell and skin (mid); and max pressure (MPa) on each face (bottom)

3.2. Validation using pressure sensors

First, 4 SingleTact sensors are placed on the silicone at strategic points, where the pressure is the greatest. The first was placed at the root of the nose (1), the second on the left corner of the nose (2), the third on the top of the right cheek (3), and the fourth in the middle of the neck below the chin (4) (see figure 6A and 6B).

Pressure tests were performed on participant 1, successively under all 3 tightening forces (5N, 13N, and 20N). The raw pressure results are extremely noisy, so it was necessary to run them through a smoothing algorithm to highlight the pressure trends. The values are presented in figure 6C.

The highest pressure is measured at the neck (4), reaching $1{,}0.10^{-2}$ MPa under a tightening of 20N. This value is of the same order of magnitude as that obtained by simulation ($2{,}1.10^{-2}$ MPa on the same participant). The lowest is the one measured at the corner of the nose, which also correlates with what is observed on the simulations. Nevertheless, the contact seems to be present at the corner of the nose because the sensor detects a pressure. This is not in agreement with what we observe from the simulations and the make-up. Finally, the other pressure values than the one obtained in (4) are even more inferior to the ones obtained by simulation at the same places.

Due to lack of time and shortage of sensors, we could not perform more tests on the other participants.

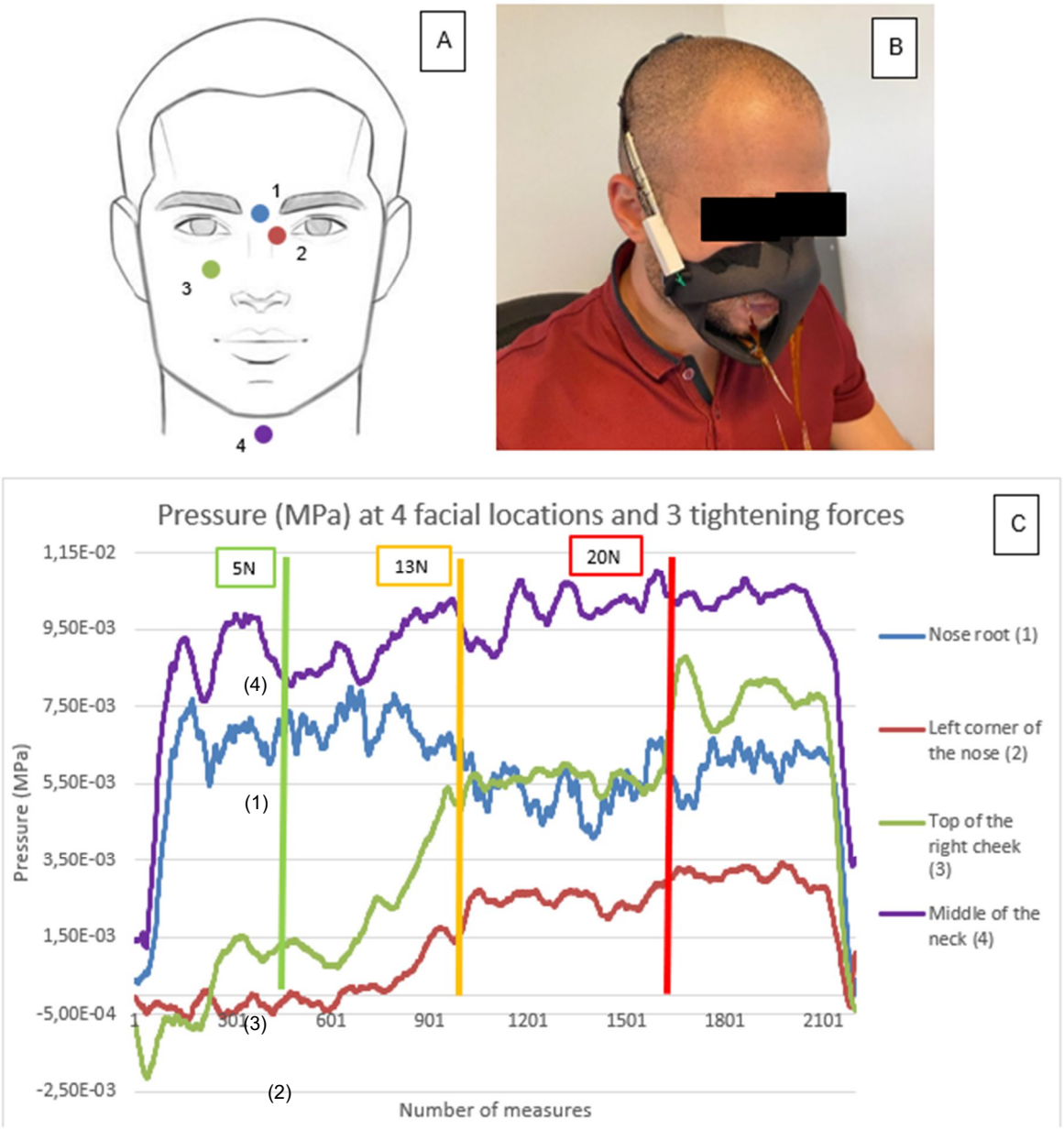

Fig. 6. Sensors' position (A); Pressure measurement on participant 1 (B); Pressure at the 4 strategic locations as a function of mask tightening force (C)

3.3. Seal validation

Validation of the mask's seal using makeup confirms the gap results from the simulation. Indeed, a gap in the black make-up is present at the corners of the nose (green circle in Fig. 7), as in the simulations. For the rest of the contour, the silicone is in good contact with the skin, which ensures a good seal.

Fig. 7. Sealing contour using make-up

4. Discussion

First simulations on a panel of 7 people have been carried out by refining the model since [13]. The experimental protocol for calculating pressure and gap in order to validate the model has been created.

The first results obtained are promising and more experimental pressure results will be available shortly. Both experimental and simulation first results are in the order of 10^{-2} – 10^{-3} MPa, which is in agreement with the literature [15]. A lower pressure on participant 7 may be linked to the fact that he was the only participant with a full beard during the scan. To the best of our knowledge, there is no data yet on whether these pressure values can have an impact on comfort and on the soft tissue of the face. The pressure peaks' values determined in the simulations will be contrasted to the measured ones. These will then be evaluated to ensure whether they are below the pain threshold, with the help of feedback and comments from participants.

The method of experimental pressure measurement by SingleTact sensors is also promising. Measurements on the other 6 participants will be done soon to verify if the pattern of values obtained with participant 1 is found on the others. Further research is needed to find out if the simulations overestimate the pressure, or if the experimental measurement method needs to be refined to improve the veracity of the measurement. The final goal is to use 8 sensors on each participant to cover more points on the face (1 on the root of the nose, 2 on each side of the nose, 2 on each cheek, as well as 3 on the neck). If the values exhibit symmetry with respect to the face's center plane, the number of sensors will be reduced in future captures.

The Gap pattern on the simulation and experiments are similar (tightness on the cheeks and neck, but gap at the nose). This analysis remains qualitative and allows to verify what is obtained by the simulations. The problem of the gap at the nose may be solved by using a newer version of the ShapeShift3D mask (Beyond-Fit™ Face mask), tightened at the nose. The fact that the participant has a beard may also reduce the visibility and reliability of the results. Participants without a beard should therefore be chosen to obtain the most reliable results possible. Otherwise, a revised version of the protocol will adapt the scanning method for participants with beards.

The mask placement/tightening process is currently being refined in the simulation to get as close as possible to the actual behavior. The experimental pressure/gap results will help fine-tune the simulation boundary conditions.

Further simulations need to be carried out to show, for example, the impact of facial soft tissue parameters, boundary conditions, and applied force. When the results are close to those obtained experimentally, the parameters of the simulation will be saved and used for all further simulations. Once validated, they will be used to train a machine learning algorithm. Training dataset will be composed of face scans with their personalized masks, and the corresponding facial deformation, gap and pressure

maps generated with finite element simulations. This will allow the pressure map to be obtained in real-time for the customer, to make sure that their mask fits their face before ordering.

Some limitations can be mentioned. First, our study is currently limited to a panel of 7 people of the same gender, age group and ethnicity. A larger number of simulations will then be carried out, thanks to the recruitment of a diverse panel (different sexes, ages, and ethnicities) of 25 participants. A total of 6 scans will be performed on each participant (3 with We3D on iPhone and 3 with the Structure Sensor on iPad). More than 150 scans will then be used as a database for the machine learning algorithm. Experimental pressure tests will also be carried out on these participants with their dedicated custom masks. As mentioned before, there is no data to our knowledge linking an amount of pressure on the face and the associated comfort/pain. Therefore, we will have the participants fill out a questionnaire asking, among other things, about their feelings about the comfort of the mask to correlate the answers to the pressure results. The simulation parameters are not yet all validated and we are still studying the influence of soft tissue properties, the orientation of the tension spring, and mask-face contact parameters on the pressure and gap results obtained. Furthermore, the qualitative gap identification methods (face makeup) would not fully ensure a seal as per NIOSH standards but will guide contact patterns outlined by the simulations. Nevertheless, these limitations will be addressed in future studies.

5. Conclusion

In this study, finite element simulations of respiratory masks fitting were conducted to evaluate primary pressure and gap. A validation protocol is presented to compare simulated results with capacitive pressure sensors to validate the model parameters. Respiratory masks adapted to each face remains an asset for workers in factories and hospitals. A personalized fitting might contribute to more comfortable experience for the user under prolonged period, while providing adequate respiratory protection

6. Acknowledgements

I would like to thank the Consortium industriel de recherche et d'innovation en technologies de la santé (MEDTEQ+) as well as the Ministère de l'Economie et de l'Innovation du Québec for their confidence and support of the project.

References

[1] ELF, “Les affections pulmonaires liées au travail,” *European Lung Foundation*. https://europeanlung.org/fr/information-hub/lung-conditions/les-affections-pulmonaires-liees-au-travail/ (accessed Aug. 19, 2022).

[2] J. Racine, “Maladies respiratoires professionnelles : évitez de mordre la poussière - Airex Industries.” https://www.airex-industries.com/fr/medias/307-maladies-respiratoires-professionnelles-evitez-de-mordre-la-poussiere (accessed Aug. 19, 2022).

[3] L. Kuo, “China confirms human-to-human transmission of coronavirus,” *The Guardian*, Jan. 21, 2020. Accessed: Aug. 19, 2022. [Online]. Available: https://www.theguardian.com/world/2020/jan/20/coronavirus-spreads-to-beijing-as-china-confirms-new-cases

[4] “How does coronavirus spread?” *NBC News*. https://www.nbcnews.com/health/health-news/how-does-new-coronavirus-spread-n1121856 (accessed Aug. 19, 2022).

[5] P. Anfinrud, V. Stadnytskyi, C. E. Bax, and A. Bax, “Visualizing Speech-Generated Oral Fluid Droplets with Laser Light Scattering,” *N Engl J Med*, vol. 382, no. 21, pp. 2061–2063, May 2020, doi: 10.1056/NEJMc2007800.

[6] “Transmission of SARS-CoV-2: implications for infection prevention precautions.” https://www.who.int/news-room/commentaries/detail/transmission-of-sars-cov-2-implications-for-infection-prevention-precautions (accessed Aug. 31, 2022).

[7] "Proper N95 Respirator Use for Respiratory Protection Preparedness | Blogs | CDC." https://blogs.cdc.gov/niosh-science-blog/2020/03/16/n95-preparedness/ (accessed Aug. 19, 2022).

[8] Y. Qian, K. Willeke, S. A. Grinshpun, J. Donnelly, and C. C. Coffey, "Performance of N95 Respirators: Filtration Efficiency for Airborne Microbial and Inert Particles," *American Industrial Hygiene Association Journal*, vol. 59, no. 2, pp. 128–132, Feb. 1998, doi: 10.1080/15428119891010389.

[9] S. Rengasamy and B. C. Eimer, "Nanoparticle Penetration through Filter Media and Leakage through Face Seal Interface of N95 Filtering Facepiece Respirators," *The Annals of Occupational Hygiene*, vol. 56, no. 5, pp. 568–580, Jul. 2012, doi: 10.1093/annhyg/mer122.

[10] H. Lee, "Effects of Long-Duration Wearing of N95 Respirator and Surgical Facemask: A Pilot Study," *Journal of Lung, Pulmonary & Respiratory Research*, vol. 1, Nov. 2014, doi: 10.15406/jlprr.2014.01.00021.

[11] U.-N. Lam, N. S. F. Md. Mydin Siddik, S. J. Mohd Yussof, and S. Ibrahim, "N95 respirator associated pressure ulcer amongst COVID-19 health care workers," *International Wound Journal*, vol. 17, no. 5, pp. 1525–1527, 2020, doi: 10.1111/iwj.13398.

[12] J. Borduas, A. Castonguay, P. Laurin, and D. Beland, "Reliability of Mobile 3D Scanning Technologies for the Customization of Respiratory Face Masks," presented at the 3DBODY.TECH 2020 - 11th International Conference and Exhibition on 3D Body Scanning and Processing Technologies, Online/Virtual, 17-18 November 2020, Online, Nov. 2020. doi: 10.15221/20.34.

[13] L. Degueldre *et al.*, "Improving the Fit of Respiratory Face Masks through 3D Scanning, Finite Elements Analysis and Additive Manufacturing," presented at the 3DBODY.TECH 2020 - 11th International Conference and Exhibition on 3D Body Scanning and Processing Technologies, Online/Virtual, 17-18 November 2020, Online, Nov. 2020. doi: 10.15221/20.33.

[14] M. Zhang and A. F. T. Mak, "In vivo friction properties of human skin," *Prosthet Orthot Int*, vol. 23, no. 2, pp. 135–141, Aug. 1999, doi: 10.3109/03093649909071625.

[15] F. Genna, N. F. Lopomo, and F. Savoldi, "Validation of a numerical model for the mechanical behavior of a continuous positive airway pressure mask," *Computer Methods in Biomechanics and Biomedical Engineering*, Sep. 2021, Accessed: Aug. 30, 2022. [Online]. Available: https://www.tandfonline.com/doi/full/10.1080/10255842.2021.1940975

[16] J. W. R. Verberne, P. R. Worsley, and D. L. Bader, "A 3D registration methodology to evaluate the goodness of fit at the individual-respiratory mask interface," *Comput Methods Biomech Biomed Engin*, pp. 1–12, Nov. 2020, doi: 10.1080/10255842.2020.1849156.